International Journal of Thermofluid Science and Technology (2024)
Volume 11, Issue 1, Paper No. 110101
https://doi.org/10.36963/IJTST.2024110101
Research Article

Aspect ratio effect on natural convection flow in a greenhouse submitted to a geothermal heat source

Yassine Slatni[1], Brahim Mahfoud[2,*], Tarek. Messai[2] , Mahfoud. Djezzar[1]

[1]*Energetic Physics Laboratory, Exact Sciences Faculty, Frères Mentouri Constantine 1 University, Algeria.*
[2]*Department of Mechanical, University of AMO-Bouira, 10000, Algeria.*

ATICLE INFO

Received: 11 Sep. 2023;
Received in revised form:
27 Oct. 2023;
Accepted: 01 Dec. 2023;
Published online:
08 Dec. 2023

Keywords:
Aspect ratio
Greenhouse
Geothermal energy
Bipolar coordinates
Nusselt number
Plant growth

ABSTRACT

The study of how greenhouse dimensions affect heat transfer and convection is pivotal in refining greenhouse design for optimal plant growth. In this context, this paper presents the aspect ratio effect on natural convection flow within a tunnel greenhouse is undertaken. During the winter season, the base of the greenhouse is subjected to geothermal energy to maintain a temperature T_h, while the roof is exposed to a lower temperature T_c. The principal flow attributes are defined by a pair of dimensionless parameters: the aspect ratio (f=K/L) and the Rayleigh number (Ra). The effects of Rayleigh number which varies from $10^3 \leq Ra \leq 10^6$ as well as the aspect ratio between $0.6 \leq f \leq 1$ were investigated. A numerical approach in bipolar coordinates is suggested, utilizing an implicit finite volume formulation.

The findings are visualized through streamlines and isotherms contours. Profiles for average and local Nusselt numbers, as well as distributions of temperature and velocity, are also presented. The conclusions indicate that in scenarios featuring minor temperature disparities between the greenhouse interior and exterior, heat transfer is predominantly governed by pseudo-conduction. However, with an increase in the temperature difference, natural convection emerges as the dominant heat transfer mechanism, leading to an enhancement in heat transfer efficiency. Moreover, the aspect ratio of the greenhouse demonstrates a proportional correlation with internal heat transfer efficiency. These insights offer valuable direction for the optimization of greenhouse design and operation.

1. Introduction

Born a little over fifty years ago, the sheltered cultivation system has nowadays become an essential tool for meeting food needs in fresh produce, because the essential function of an agricultural greenhouse is to create a more favorable to the requirements of

*Corresponding e-mail: b.mahfoud@univ-bouira.dz (Brahim Mahfoud)

Nomenclature

A	Focal distance, coefficient	x,y	Cartesian co-ordinates, m
D	Characteristic longer, m	*Greek symbols*	
F	Function	α	Thermal diffusivity, m²/s
F	Aspect ratio	β	Thermal expansion coefficient, (1/K)
G	Function	η	Vertical bipolar coordinate
Gr	Grashof number, $Gr = Ra / \Pr$	θ	Horizontal bipolar coordinate
G	Gravity acceleration, m.s^{-2}	ν	Cinematic viscosity, m²/s
H	Dimensionless metric Coefficient	ψ^*	nondimensional stream function
H	Dimensional metric Coefficient, m	ω	Vorticity, s^{-1}
K	Height of the tunnel greenhouse,m	*Subscripts*	
L	Greenhouse width,m	av	Average
NI	The total number of nodes following η	l	Local
NN	The total number of nodes following θ	C	Cold
Nu_{av}	Average Nusselt number	H	Hot
Nu_l	Local Nusselt number	max	The maximum value
Nt	Number of tubes	i	The variation along the axis η
Pr	Prandtl number, $\Pr = \nu / \alpha$	j	The variation along the axis θ
Ra	Rayleigh number, $Ra = g\beta\Delta TL^3 / \nu\alpha$	*Superscripts*	
T	Dimensional temperature, K	*	Dimensionless
u,v	Dimensional velocity-components, m.s^{-1}		

the plant as the local or regional climate. Within greenhouse environments, natural convection is a significant physical phenomenon. Several studies have explored various aspects of this convection within differently shaped enclosures. For instance, Fayz-Al-Asad et al. [1] investigated natural convection in a wavy cavity featuring a single horizontal fin on its hot wall. In a similar vein, Haithem et al. [2] delved into heat transfer in a horizontal annulus equipped with both longitudinal and transversal fins on its inner surface. Dogonchi et al. [3] focused on the free convection of a copper-water nanofluid in the upper half of a circular horizontal cylinder. Sheremet and Pop [4] conducted a numerical investigation into natural convection and heat transfer in a concentric horizontal annulus. These studies collectively provide valuable insights into the behavior of natural convection within specific greenhouse-related configurations, shedding light on critical factors influencing heat transfer and fluid flow. For the greenhouse the natural convection mode is affected in turn by the change of greenhouse geometry. Several studies have been done in this area by several researchers. Draoui et al. [5-6] conducted a numerical investigation into both Laminar and Transient natural convection within a single-span greenhouse that was heated from beneath. They highlighted that when certain conditions, such as flow constraints at the ground level and a lower temperature at the roof, were imposed; a temperature contrast came into play, initiating an air circulation featuring two counter-rotating vortices. Furthermore, by introducing a pressure variance between the floor and the ceiling, they observed a positive contribution to efficient air circulation throughout the greenhouse. Bouali et al. [7] and Dihmani et al. [8] conducted numerical investigations focusing on heat transfer and air-flow within a greenhouse. The outcomes of their studies demonstrated that by optimizing the shape of solid structures, heat transfer within the greenhouse can be significantly enhanced. The numerical simulation of heat transfer in a greenhouse, which was heated by tubes positioned underground, was discussed in the work of Mezrhab et al. [9]. The authors explored the impact of varying the number of tubes (Nt) on the thermal dynamics within the

greenhouse. Notably, they observed a substantial influence of (Nt) on thermal behavior, particularly evident within a range of values where $10^3 \leq Ra \leq 10^6$. Furthermore, as the number of heating tubes increased, the average Nusselt number emerged as another crucial parameter indicative of heat transfer efficacy within the greenhouse, especially at elevated Rayleigh number values. Ghosal and Tiwari. [10] They used geothermal energy and a thermal curtain to heat a single-chapel greenhouse. They found that the best range of air temperature around a bouquet, during a cold winter night and at dawn between 14 and 23°C, this translates to better winter plant growth.

Recent advancements in optimizing energy efficiency within greenhouse control operations and energy simulations have prompted various approaches. Iddio et al. [11] delved into strategies targeting enhanced energy efficiency through the controlled manipulation of critical greenhouse parameters, concurrently developing a network for detection and monitoring systems. Furthermore, they compiled an encompassing review that synthesized both established and evolving methodologies in the realm of greenhouse energy modeling.

In a similar vein, Van Henten and Bontsema [12] explored the interrelation between control resolution and quantifiable energy conservation. Their findings indicated that adopting a heating profile resolution spanning from half an hour to one-hour yields sufficiently accurate outcomes in terms of energy preservation.

In their research, Taki et al. [13] extensively explored pivotal strategies for energy-saving technologies, centering around the simulation of heat and mass transfer, as well as incorporating artificial intelligence for climate control. Their investigation predominantly encompassed innovative and sustainable solutions grounded in renewable resources. These solutions featured photovoltaic (PV) modules, solar thermal collectors (T), as well as integrated (PV/T) hybrid systems.

In the same context of greenhouse heating and convection, a previous study by Slatni et al. [14] conducted a numerical investigation on natural convection in a double chapels greenhouse. The impact of the Grashof number on the natural convection phenomena within the greenhouse was explored. Ultimately, the simulation results were presented as stream function lines and temperature fields. Moreover, in a separate investigation led by Slatni et al. [15], the focus remained on scrutinizing the implications of the Rayleigh number on heat transfer. Under the reference conditions where the number of tubes was held constant (Nt=3), the augmenting Rayleigh number and the increased count of tubes (Nt) synergistically amplified the prevalence of natural convection. This effect subsequently led to a discernible enhancement in heat transfer efficiency. Broadly speaking, the upsurge in heat transfer exhibited a direct correlation with the escalating number of tubes, effectively underscoring the constructive role of tube count in shaping the dynamics of heat exchange. As greenhouse temperatures rise, the need arises to facilitate ventilation, achieved either naturally or through artificial means. In pursuit of this objective, a numerical simulation was undertaken to comprehend the thermal dynamics of a naturally ventilated greenhouse, as carried out by Slatni et al. [16]. The outcomes of this investigation illuminate that optimal heat exchange between the greenhouse's interior air and the external atmosphere is achieved through ventilation at the upper aperture. This ventilation strategy plays a pivotal role in maintaining a favorable climate conducive to plant growth, thereby safeguarding their development.

Considerable research has been dedicated to greenhouse energy modeling in recent times, propelled by advancements in computational power. Nonetheless, only a fraction of these studies have explored the modeling of heat transfer within greenhouses of varying sizes. In this study we are interested in the influence of the height/width ratio of a greenhouse on the convection generated by a geothermal heat source below. The question is that the height/width ratio of a greenhouse can indeed have a significant impact on heat transfer and energy efficiency.

2.Physical Modeling and Governing equations

Fig.1 displays a cross-sectional plan of a two-dimensional layout for the greenhouse under consideration. The model system depicted schematically in Fig.1 is a flat semi-circle filled with air (Pr=0.7), which is considered incompressible, laminar, and stationary. The greenhouse has the dimensions of length L and varied height K. The base of the greenhouse is subjected to geothermal energy, which is maintained at a high-temperature T_h, while the roof is at a low temperature $T_c<T_h$. The radial temperature gradient is produced by the temperature difference between T_c and T_h. The geometric configuration lends itself well to description through the utilization of the bipolar coordinate system (η, θ), as illustrated in Fig.2. The transformation equations from the conventional Cartesian coordinate system (x, and y) to the bipolar coordinate system are presented below.

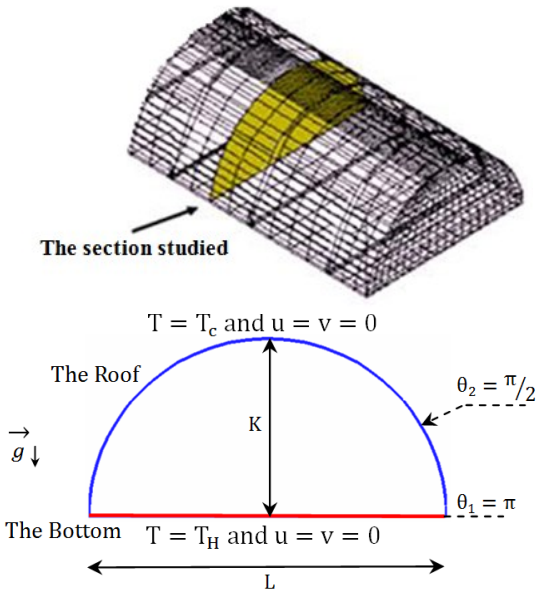

Fig. 1 Schematic representation of a tunnel greenhouse heated from below.

2.1 Simplifying assumptions

A system of interconnected and nonlinear partial differential equations was encountered by us. The resolution of such a system, inclusive of a specific set of initial and boundary conditions, is posed as a formidable challenge. To render this task more manageable and the resolution process more streamlined, several approximations and simplifying assumptions were introduced:

-The adherence of the fluid, air in this case, to the characteristics of a Newtonian and viscous fluid was assumed by us.

-The simplifying assumption of the fluid being incompressible was made.

-Constants were used in our analysis for the thermo-physical properties of the fluid.

-Insignificant nature was attributed to viscous dissipation due to the relatively low velocities involved in the system.

-Negligibility was assigned to the heating power generated by compression in comparison to other energy-related terms.

-Approximating the density of the fluid as varying linearly with temperature and concentration.

The equations expressing the flow phenomena are mainly those derived from the physical laws of conservation of mass, momentum, and energy, in cartesian coordinates, and are written using the stream function and vorticity, cited as follows:

$$\frac{\partial^2\psi}{\partial x^2}+\frac{\partial^2\psi}{\partial x^2}=-\omega \tag{1}$$

$$u\frac{\partial T}{\partial x}+v\frac{\partial T}{\partial y}=\alpha\left(\frac{\partial^2 T}{\partial x^2}+\frac{\partial^2 T}{\partial y^2}\right) \tag{2}$$

$$u\frac{\partial \omega}{\partial x}+v\frac{\partial \omega}{\partial y}=g\beta\frac{\partial T}{\partial x}+\nu\left(\frac{\partial^2 \omega}{\partial x^2}+\frac{\partial^2 \omega}{\partial y^2}\right) \tag{3}$$

With:

$$\omega=\frac{\partial v}{\partial x}-\frac{\partial u}{\partial y};\quad u=\frac{\partial \psi}{\partial x};\quad v=-\frac{\partial \psi}{\partial x} \tag{5}$$

It is convenient to define a reference frame such that the limits of the system result in constant values of the coordinates. The so-called Bipolar coordinates allow, precisely in our case, to obtain this result in Fig.2. Thereafter we use a transformation for the transition from the cartesian coordinates (x,y) to the Bipolar coordinates (η,θ) [17].

$$\begin{cases} x = \dfrac{a.\sinh(\eta)}{(\cosh(\eta)-\cos(\theta))} \\ y = \dfrac{a.\sin(\theta)}{(\cosh(\eta)-\cos(\theta))} \end{cases} \quad (6)$$

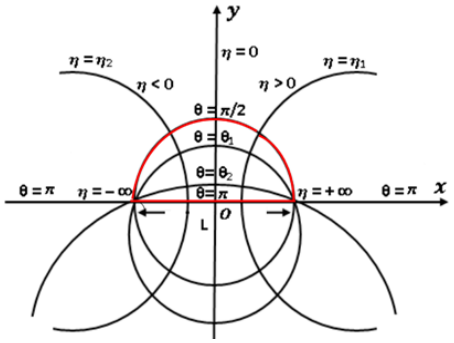

Fig. 2 Schematic representation of bipolar coordinates.

The relations from (2) to (4) are then written respectively:

$$\frac{\partial^2\psi}{\partial\eta^2}+\frac{\partial^2\psi}{\partial\theta^2}=-h^2\omega \quad (7)$$

$$V_\eta\frac{\partial T}{\partial\eta}+V_\theta\frac{\partial T}{\partial\theta}=\alpha\left(\frac{\partial^2 T}{\partial\eta^2}+\frac{\partial^2 T}{\partial\theta^2}\right) \quad (8)$$

$$V_\eta\frac{\partial\omega}{\partial\eta}+V_\theta\frac{\partial\omega}{\partial\theta}=\frac{\nu}{h}\left(\frac{\partial^2\omega}{\partial\eta^2}+\frac{\partial^2\omega}{\partial\theta^2}\right)+ g\beta\left(F(\eta,\theta)\frac{\partial T}{\partial\eta}-G(\eta,\theta)\frac{\partial T}{\partial\theta}\right) \quad (9)$$

With:

$$\begin{cases} V_\eta = \dfrac{1}{h}\dfrac{\partial\psi}{\partial\theta} \\ V_\theta = -\dfrac{1}{h}\dfrac{\partial\psi}{\partial\eta} \end{cases}, \quad \omega = -\frac{1}{h^2}\left(\frac{\partial^2\psi}{\partial\eta^2}+\frac{\partial^2\psi}{\partial\theta^2}\right) \quad (10)$$

$$h=\frac{a}{(\cosh(\eta)-\cos(\theta))} \quad (11)$$

$$\begin{cases} F(\eta,\theta) = \dfrac{1-\cosh(\eta)\cos(\theta)}{(\cosh(\eta)-\cos(\theta))} \\ G(\eta,\theta) = \dfrac{\sinh(\eta)\sin(\theta)}{(\cosh(\eta)-\cos(\theta))} \end{cases} \quad (12)$$

Introducing the following dimensionless variables:

$$D_h=a; H=\frac{h}{D_h}; V_\eta^*=V_\eta\frac{D_h}{\alpha}; V_\theta^*=V_\theta\frac{D_h}{\alpha}; \psi^*=\frac{\psi}{\alpha};$$

$$\omega^*=\omega\frac{D_h^2}{\alpha}; T^*=\frac{T-T_c}{T_h-T_c}.$$

Then the equations (7), (8), and (9) become:

$$\frac{\partial^2\psi^*}{\partial\eta^2}+\frac{\partial^2\psi^*}{\partial\theta^2}=-H^2\omega^* \quad (13)$$

$$V_\eta^*\frac{\partial T^*}{\partial\eta}+V_\theta^*\frac{\partial T^*}{\partial\theta}=\frac{1}{H}\left(\frac{\partial^2 T^*}{\partial\eta^2}+\frac{\partial^2 T^*}{\partial\theta^2}\right) \quad (14)$$

$$V_\eta^*\frac{\partial\omega^*}{\partial\eta}+V_\theta^*\frac{\partial\omega^*}{\partial\theta}=\frac{\Pr}{H}\left(\frac{\partial^2\omega^*}{\partial\eta^2}+\frac{\partial^2\omega^*}{\partial\theta^2}\right)+ \Pr.Ra\left(F(\eta,\theta)\frac{\partial T^*}{\partial\eta}-G(\eta,\theta)\frac{\partial T^*}{\partial\theta}\right) \quad (15)$$

The dimensionless boundary conditions

- At the Bottom:

$$V_\eta^*=V_\theta^*=0;\omega^*=\frac{1}{H^2}\left(\frac{\partial^2\psi^*}{\partial\eta^2}+\frac{\partial^2\psi^*}{\partial\theta^2}\right)=0;T=T_H \quad (16)$$

$$\psi^*(\eta,\theta)\big|_{\theta=\theta_1}=0 \quad (17)$$

- At the Roof:

$$V_\eta^*=V_\theta^*=0;\omega^*=\frac{1}{H^2}\left(\frac{\partial^2\psi^*}{\partial\eta^2}+\frac{\partial^2\psi^*}{\partial\theta^2}\right)=0;T=T_C \quad (18)$$

$$\psi^*(\eta,\theta)\big|_{\theta=\theta_2}=0 \quad (19)$$

In addition to displaying the natural convection flow through streamlines and isotherms, we show you the average Nusselt number for clearer interpretation, which is defined as follows:

$$Nu_{av}=\frac{1}{(\eta_{NI}-\eta_1)}\int_{\eta_1}^{\eta_{NI}}Nu\,\partial\eta=\frac{1}{(\eta_{NI}-\eta_1)}\sum_{i=1}^{i=NI}Nu_i \quad (20)$$

The local Nusselt number is defined as:

$$Nu_l=-\frac{1}{H}\left(\frac{\partial T^*}{\partial\theta}\right)_{\theta=\theta_1} \quad (21)$$

3. Procedure, numerical method and validation

In this part, Fig.3 represents the physical domain and the computational domain. The equations expressing the flow phenomena are mainly those derived from the physical laws of

conservation of mass, momentum, and energy (13)–(15), as well as the boundary conditions (16) to (19) were processed using the finite volume method [18-23]. The two diffusive and convective terms of the energy and vorticity equations are treated respectively one by a central differentiation scheme [24-26]. and the other by a power law differentiation scheme [27-30].

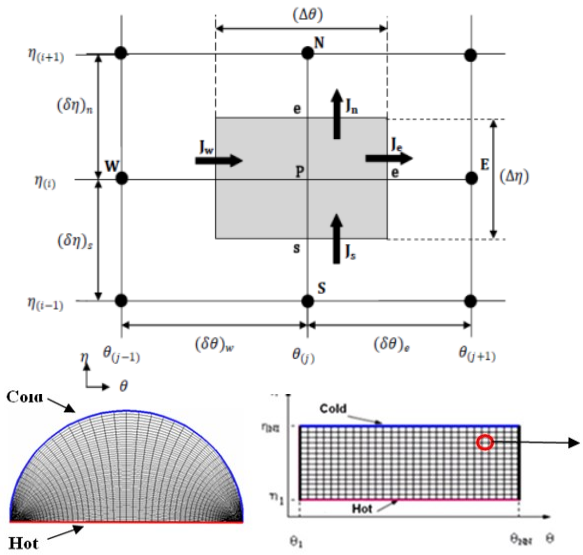

Fig. 3 Grids domain and the computational domain.

3.1. Grid independence study

All the results presented in this paper have been obtained using four grids, each corresponding to one of the four cases studied here (f=1, 0.95, 0.8, and f=0.6, respectively). The solution domain comprises a two-dimensional non-uniformly spaced staggered grid. Grid dependency has also been tested in this study using the average Nusselt number in the case of Ra=10^5. The results shown in Fig.4 indicate that a grid size of N_η segments in the η-direction and N_θ segments in the θ-direction ensures grid independence for f=0.6, 0.8, 0.95, and f=1.0, respectively. The mesh sizes chosen are (70×70), (70×80), (70×85), and (70×85) for f=0.6, 0.8, 0.95, and f=1.0, respectively, based on several numerical tests conducted. The convergence criterion involves reducing the maximum mass residual of the grid control volume to below 10^{-6}. This criterion required a few CPU seconds per step on a main frame workstation with 128 GB of RAM.

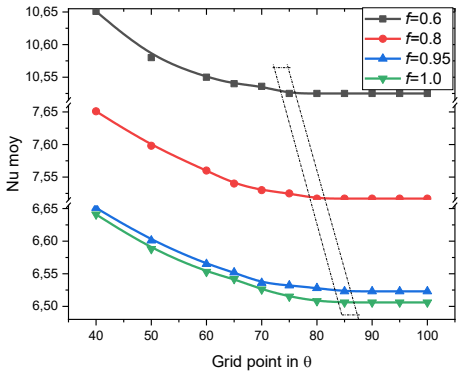

Fig. 4 Grid dependency for Ra = 10^5

3.2. Code validation

To validate the accuracy of our computer code, we cross-referenced our findings with preexisting data acquired by Kabdi et al. [23]. This validation process entailed conducting numerical 2D simulations on an enclosure defined by the intersection of two cylindrical walls. The scenario involved heat flow emanating from the base of one wall while the opposite wall served as the cooler roof, featuring varied geometry sizes. The outputs of case Pr=0.7, Gr=2.10^6 shown in Fig.5 demonstrated a notable concurrence between our results and theirs, affirming a high level of agreement.

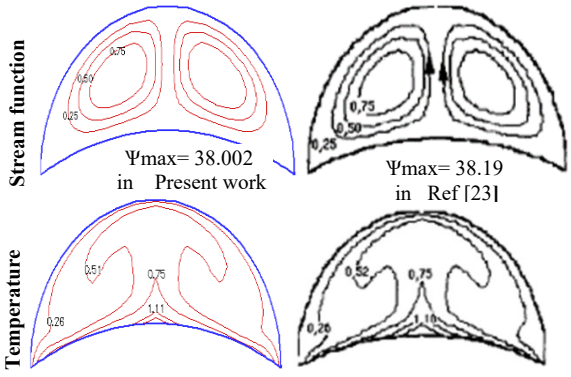

Fig. 5 Comparison of streamlines and isotherms of present work with reference [23].

4. Results and Discussion

The calculations were conducted for a fluid with a Prandtl number of 0.71 within a semicircular domain characterized by various aspect ratios: $f=K/L=1$, 0.95, 0.8, and 0.6. The aspect ratio $f=1.0$ was selected as the reference due to its representation of a half-circle geometry. Additionally, the outcomes of the free convection phenomena were acquired for diverse geometries corresponding to the four mentioned cases, as depicted in Fig.6. Because of the applied temperature gradient between the roof and the base and the absence of pressure variations in the two transverse directions ($\partial P/\partial \eta = \partial P/\partial \theta = 0$), the dimensionless Rayleigh number becomes an explicit necessity for arriving at a solution.

The objective of this study in this section for a closed greenhouse is to examine the influence of the Rayleigh number ($10^3 \leq Ra \leq 10^6$) and that of the aspect ratios ($0.6 \leq f \leq 1$), when the number of Prandtl is fixed at 0.71, on the flow and the transfer of heat inside the greenhouse. The results are presented in the form of streamlines and isotherms, as well as in terms of variations in the average Nusselt number and the distribution of temperature and velocity, for different vertical positions chosen inside the greenhouse.

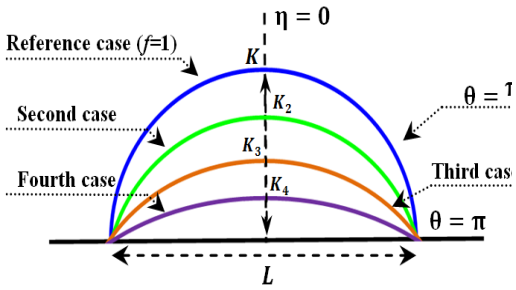

Fig. 6 Greenhouse with different heights.

4.1. Buoyancy effect on the behavior of the fluid layers and thermal field

To investigate the effects of thermal gradients on the fluid layers and thermal field (Streamlines, and isotherms), four Rayleigh numbers $Ra=10^3, 10^4, 10^5$ and 10^6 are compared with reference case ($f=1$).

For $Ra=10^3$ shown in Fig. 7, we notice the presence of two counter-rotating vortices, of large sizes, on the left side the flow turns clockwise, and on the right side in the opposite direction because of the shape of the greenhouse. The value of the current function for this case is very small $\psi^*_{max}=0.104$, also the velocity fields are different from zero $V^*_{\eta_{max}}=0.358$; $V^*_{\theta_{max}}=0.417$. So with this situation, the heat transfer is by pseudo conduction. When the Rayleigh number is increased to 10^4, a slight change in the streamlines is noticed, as the centers of the two vortices shift slightly toward the middle of the greenhouse. This development is accompanied by a slight increase in the value of the streamlines to be equal to $\psi^*_{max}=2.467$ and $V^*_{\eta_{max}}=8.788$; $V^*_{\theta_{max}}=11.32$. This reflects a transformation from conductive transfer to convective transfer, but it remains relatively weak. When we raise the value of the Rayleigh number to $Ra=10^6$, the figure illustrates a flow characterized by two vortices occupying almost the entire greenhouse, this shows that the exchange is convective. The values of the maximum velocities increase significantly for $Ra=10^6$ where $V^*_{\eta_{max}}=195.8$; $V^*_{\theta_{max}}=234.1$ and of the current function $\psi^*_{max}=44.77$.

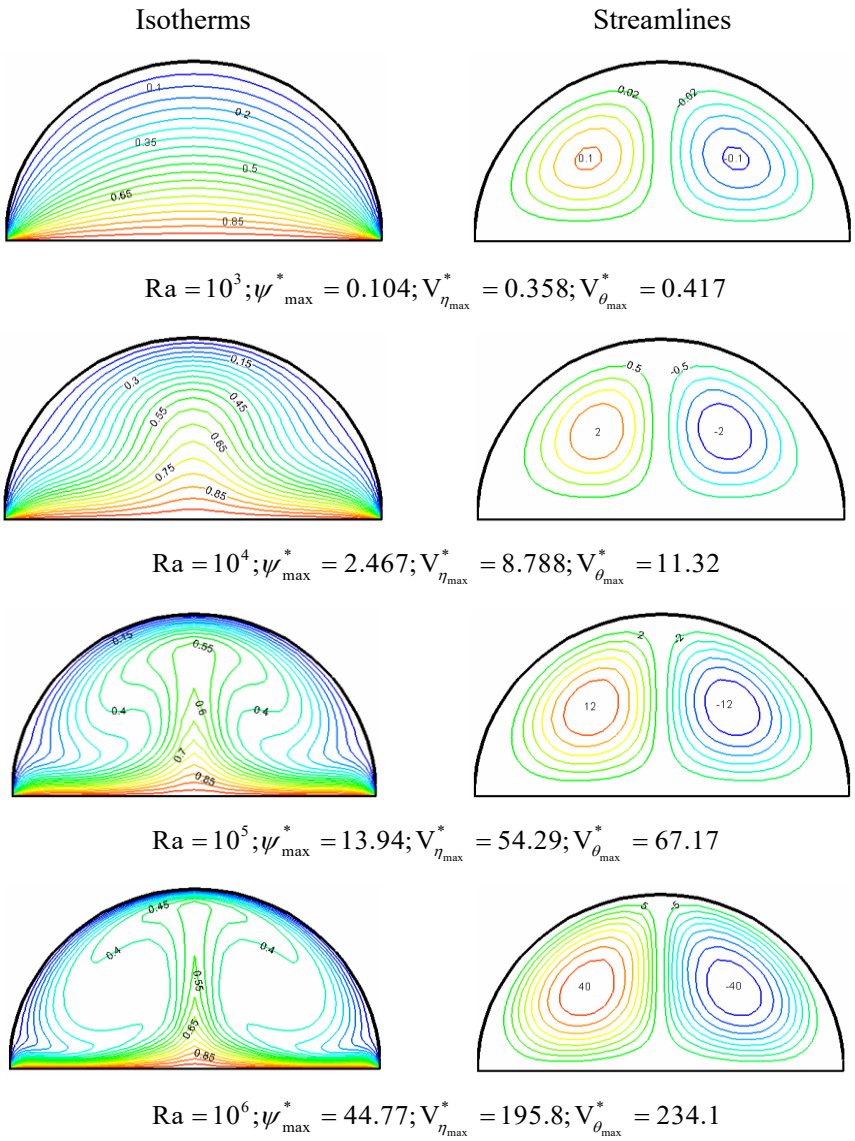

Fig. 7 Isothermal lines and streamlines for f=1 at different values of Rayleigh numbers.

Also for the isotherms, if Ra=10^3, the almost parallel curves gradually take the profile of the roof, that is to say, that the temperature distribution is simply decreasing from bottom to top. We can say that heat transfers are done by pseudo-conduction. With the increase of the number of Rayleigh, the isothermal lines are modified appreciably, which translates the transformation towards the convective mode. Whereas for large Rayleigh values, the isothermal lines change and eventually adopt the shape of a mushroom or the direction of the deformation of the isotherms is by the direction of rotation of the streamlines, which means that the dominant convection mode.

4.2. Aspect ratio effect on natural convection in the greenhouse

The general increase in the height and volume of the greenhouse throughout the world, particularly in hot regions [20]. This parameter has serious consequences on the condition of the indoor climate. To study this point more thoroughly, we simulated the

indoor climate of three identical agricultural greenhouses (basic type presented previously) differing only in their height, under similar climatic conditions.

For this reason, we have analyzed the effect of the height and the number of the Rayleigh on the convection in the greenhouse (see Fig. 8). The results obtained in the form of isotherms, streamlines, the local and average Nusselt number, as well as temperature and speed curves are illustrated. The effect of the geometry appears, when the space between the bottom and the roof, decreases, that is to say that f=0.95, which reflects the presence of two counter-rotating vortices in the middle of the greenhouse, with a decrease in the value of ψ^*_{max}=27.89 at Ra=10^6 even for the maximum velocities $V^*_{\eta_{max}}$=156.9; $V^*_{\theta_{max}}$=167.7 , we can therefore conclude that the natural convection in the greenhouse is less than that of the base geometry. In simulations of the geometry f=0.8, we notice a tightening of the isothermal lines in the left and right corners of the greenhouse, and this is due to the walls which are very close in these places, which favors a conductive transfer. For the case of f=0.6, there is therefore a clear decrease in the height of the greenhouse, which brings the roof of the greenhouse closer to the bottom, The isothermal lines become almost parallel in the two corners of the greenhouse, this configuration favors a better transfer by conduction in these regions and therefore the appearance of two dead zones which become more important compared to those already seen for f=0.8.

Overall we can say that the intensity of natural convection decreases as indicated by the values of the current function which decrease significantly compared to the geometries seen previously.

4.3. Temperature and velocity distribution

Two axes η=0 and η=6 have been selected for a more in-depth study on the distribution of temperature and speed inside the greenhouse (see Fig.9), plotted for case Ra=10^6 and different aspect ratios.

On the η=0 axis, the temperature profile (Fig.9.a) decreases uniformly from the bottom to the roof. This results in the stacking of isothermal lines close to the roof of the greenhouse. The velocity (Fig.9.c) is maximum on this axis, we can note a symmetrical movement with a maximum value for the case of f=1, when the velocity reaches a value of 234.1.

As for the η=6 axis, the temperature profile (Fig.9.b) the convection mode is predominant for the reference case, but for the geometry f=0.6 the shape becomes almost linear, which means that the mode is conductive. The velocities in (Fig.9.d) indicated in the same axis have a remarkable sinusoidal movement reaching a maximum of 53.55 in ultimate value.

4.4. Heat transfer

In addition to isothermal and streamlines structures, As an additional key parameter to give more explanatory information on the influence of the studied parameters (Ra and f) on the heat flow inside the greenhouse. The Nusselt number is used to characterize the type of heat transfer; it relates transfer by convection to transfer by conduction. For this reason, the average and local Nusselt numbers are presented in Figs. 10.

Fig. 10(a) displays the local Nusselt profile for different cases with the Rayleigh number equal to 10^6. We noticed that there is a similarity between the local Nusselt profile, where the curves decrease in a symmetrical way to settle in the range of L∈[-4, 4] and then decrease to a maximum value of 530.89 for case f=0.6.

Fig. 10(b) shows the average Nusselt number, it is observed that for Ra=10^4, the profile is almost linear, which reflects that the heat transfer takes place by conduction. With increasing Rayleigh number average Nusselt number also increases to reach a maximum value of 11.92, and natural convection becomes more instances.

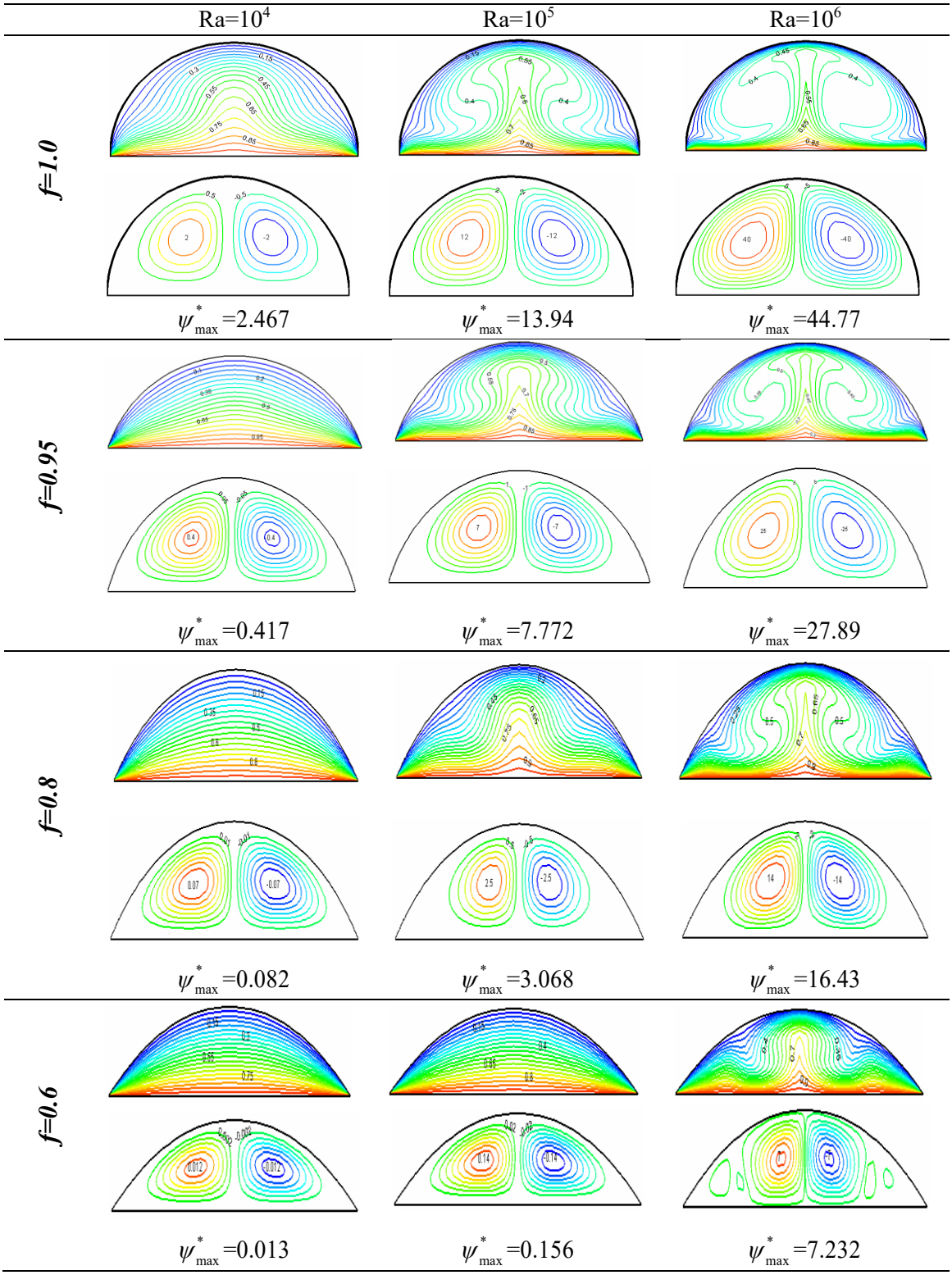

Fig.8 Isothermal and streamlines for different aspect ratios and Rayleigh number.

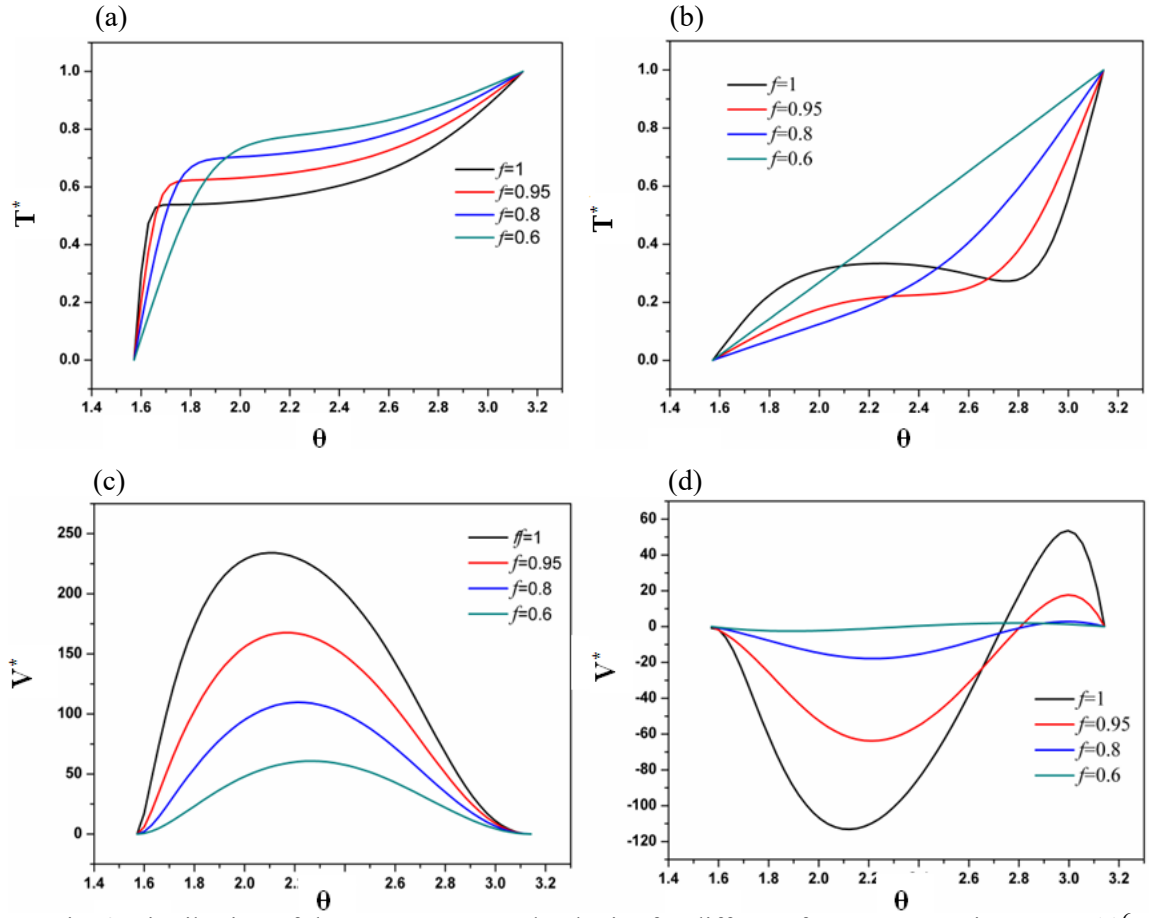

Fig. 9 Distribution of the temperature and velocity for different form aspect ratios at Ra=10^6.

5. Conclusion

The change in the geometry of the greenhouse and the temperature difference from one region to another has a significant impact on the convection inside the greenhouse. Through this, we have made a numerical study of the natural convection in a tunnel greenhouse, via governing equations formulated in bipolar coordinates and translated algebraically by the FVM method. The expression parameters for each of the greenhouse sizes and internal temperatures are the form factor and the Rayleigh number. To this end, the influence of these two parameters on the flow and heat transfer in greenhouses has been studied. Here are the most important conclusions drawn from this parametric study:

- A proportional relationship between the Rayleigh number and the flux inside the greenhouse, because the increase in the Rayleigh number better improves the heat transfer between the floor of the greenhouse and its roof to provide a favorable atmosphere for the plant.
- a proportional relationship between the Rayleigh number and the convective transfer, where for f=1 (reference case) and Ra varies from 10^3 to 10^6 there is a convective change reaching 116%.
- Greenhouse engineering has an economic and financial impact and is related to the type of plant. It turns out that the airflow and temperature inside the greenhouse are strongly affected by the height of the greenhouse. As the heat transfer is increased by increasing the form factor.

- the decrease in Aspect ratio from *f*=1 to *f*=0.6 and despite the increase in the number of Ra the convective transfer will be weaker to reach just 14% for the case of *f*=0.6 which means that the change will be almost conductive
- The shape of the average Nusselt number as a function of a lower form factor and for a large temperature difference is almost linear. But with the increase in the height of the greenhouse, the heat transfer in the greenhouse becomes more intense.

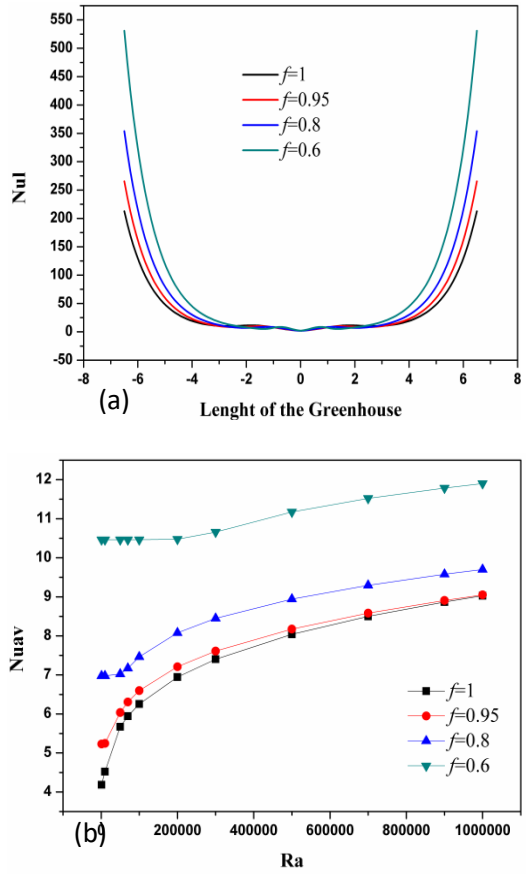

Fig. 10 Local Nusselt profile (above) and average and local Nusselt number (lowest).

References

[1] Md. Fayz-Al-Asad, M. J. H. Munshi, Md. M.A. Sarker, Effect of Fin Length and Location on Natural Convection Heat Transfer in a Wavy Cavity, Rev. International Journal of Thermofluid Science and Technology 7 (3)(2020), Paper No. 070303.

[2] H. Haithem, S. Touahri1, T. Boufendi, Conjugate heat transfer in an annulus with heated longitudinal and transversal fins, International Journal of Thermofluid Science and Technology 10, (2) (2023) Paper No. 100204.

[3] A.S. Dogonchi, M.A. Sheremet, I. Pop, D.D. Ganji, MHD natural convection of Cu/H2O nanofluid in a horizontal semi-cylinder with a local triangular heater, International Journal of Numerical Methods for Heat & Fluid Flow, 28 (12) (2018) 2979-2996.

[4] M.A. Sheremet, I. Pop, Natural convection in a horizontal cylindrical annulus filled with a porous medium saturated by a nanofluid using Tiwari and Das' nanofluid model, Eur. Phys. J. Plus 130(6) (2015) 107.

[5] B. Draoui, M. Benyamine, Y. Touhami, B. Tahri, Numerical Simulation of Natural Convection in Transient Laminar Regime in a Bottom-Heated Tunnel Greenhouse (Flow), Rev. Energ. Ren.(1999) 141–145,

[6] B. Draoui, M. Benyamine, R. Taïbi, O. Hami, Numerical Simulation of Natural Convection in Laminar and Transient Regime of a Bottom-Heated Single-Span Greenhouse (Flow), Rev. Energ. Ren. (2000)67–73,

[7] H.Bouali, A.Mezrhab, L.Elfarh, C.Abid, M.Medale.Numerical simulation of thermal transfers in an agricultural greenhouse heated by an isothermal solid block. 13th International Thermal Days, JITH 2007, Albi : France (2007).

[8] N. Dihmani, H. Bouali, A. Mezrhab, L. Elfarh, Numerical simulation of heat transfers in an agricultural greenhouse heated by solid isothermal blocks, Rev. Renewable Energy (2007) 221–224.

[9] A. Mezrhab, L. Elfarh, H. Naji, D. Lemonnier, Computation of surface radiation and natural convection in a heated horticultural greenhouse, Appl. Energy 87(3) (2010) 894–900,

[10] M.K. Ghosal, G.N. Tiwari, Mathematical modeling for greenhouse heating by using thermal curtain and geothermal energy. Solar Energy 76 (2004) 603–613.

[11] E. Iddio, L. Wang, Y. Thomas, G. McMorrow, A. Denzer, Energy efficient operation and modeling for greenhouses: A literature review, Renewable and Sustainable Energy Reviews 117 (2020) 109480,

[12] Van Henten EJ, Bontsema J. Open-loop, Optimal temperature control in greenhouses. Int Symp High Technol Greenh Syst Manag: Greensys 801(2007) 629–36.

[13] M. Taki, A. Rohani, M. R.Joneidabad, Solar

thermal simulation and applications in greenhouse. Inf Process Agric (5) (2018) 83–113.

[14] Y. Slatni, M. Djezzar, T. Messai, Numerical Investigation Of Natural Convection With Heated Tubes In Tunnel Greenhouse 7 (4) (2021) 731 – 745.

[15] Y. Slatni, M. Djezzar, R. Benderradji, Numerical study of natural convection in double chapels agricultural greenhouse. http://depot.umc.edu.dz/handle/123456789/13441.

[16] Y. Slatni, M. Djezzar, T. Messai, B. Mahfoud, Numerical simulation of thermal behavior in a naturally ventilated greenhouse, International Journal of Computational Materials Science and Engineering 11 (2022) 2150034.

[17] P. Lucht, Bipolar Coordinates and the Two-Cylinder Capacitor 53(2015) June 15, pp. 1–71.

[18] S. Patankar, Numerical heat transfer and fluid flow: Computational methods in mechanics and thermal science, Hemisphere Publication Corporation,Washington, DC. pp. 1–197, (1980).

[19] B. Mahfoud, Effect of Wall Electrical Conductivity on Heat Transfer Enhancement of Swirling Nanofluid-Flow, Journal of Nanofluids 12 (2) (2023) 418-428.

[20] B. Mahfoud, Enhancement Heat Transfer of Swirling Nanofluid Using an Electrical Conducting Lid, Journal of Thermophysics and Heat Transfer 37(1) (2023) 263–271.

[21] B. Mahfoud, Simulation of Magnetic Field Effect on Heat Transfer Enhancement of Swirling Nanofluid, International Journal of Computational Materials Science and Engineering 11(4)(2022) 2250007.

[22] H. Benhacine, B. Mahfoud, M. Salmi, Stability of conducting fluid flow between coaxial cylinders under thermal gradient and axial magnetic Field, International Journal of Thermofluid Science and Technology 9 (2)(2022) 090202.

[23] M. Fateh , B. Mahfoud, Hibet Errahmane Mahfoud, Influences of electrical conductivity of the cylindrical walls on heat transfer enhancement of nanofluid swirling flow, International Journal of Thermofluid Science and Technology 10 (2023)(2) 100201.

[24] B. Mahfoud, M. Moussaoui, Effects of buoyancy force and magnetic field on laminar vortex breakdown and fluid layers, Journal of Thermal Engineering 9 (1)(2023) 12–23.

[25] M. O. Azzoug, B. Mahfoud , Hibet. E. Mahfoud , Influence of External Magnetic Field on 3D Thermocapillary Convective Flow in Various Thin Annular Pools Filled with Silicon Melt, Journal of Applied Fluid Mechanics 16 (9)(2023)1853-1864,

[26] B. Mahfoud , M. O. Azzoug, MHD effect on the thermocapillary silicon melt flow in various annular enclosures, Crystal Research & Technology 58(6) (2023)

[27] B. Mahfoud, A. Laouari A. Hadjadj and H. Benhacine, Counter-rotating flow in coaxial cylinders under an axial magnetic field, European Journal of Mechanics-B/Fluids 78(2019) 139-146

[28] A. Bendjaghlouli, B. Mahfoud, L. Bouragbi, Magnetohydrodynamic counter rotating flow and heat transfer in a truncated conical container, Journal Thermophysics and Heat Transfer,33(3) (2019) 865-874.

[29] A, Bendjaghlouli, B. Mahfoud, and D. E. Ameziani (2019b). Magnetohydrodynamic flow in a truncated conical enclosure, Journal of Thermal Engineering 5(2019)77-83.

[30] B, Mahfoud, A. Bendjaghloli, Natural convection of a nanofluid in a conical container, Journal of Thermal Engineering 4(1)(2018)1713-1723.